Cancer Letters 457 (2019) 10–19

Contents lists available at ScienceDirect

Cancer Letters

journal homepage: www.elsevier.com/locate/canlet

Original Articles

BIRC5 is a target for molecular imaging and detection of human pancreatic cancer

Shi-He Liu[a,b], Yeahwa Hong[a], Stephen Markowiak[a], Robbi Sanchez[d], Justin Creeden[a,b], John Nemunaitis[c], Andrea Kalinoski[a], James Willey[c], Paul Erhardt[e], Jason Lee[f,g,h], Michael van Dam[f,g,h], F. Charles Brunicardi[a,b,*]

[a] Department of Surgery, University of Toledo College of Medicine and Life Sciences, Toledo, OH, 43614, USA
[b] Department of Cancer Biology, University of Toledo College of Medicine and Life Sciences, Toledo, OH, 43614, USA
[c] Department of Medicine, University of Toledo College of Medicine and Life Sciences, Toledo, OH, 43614, USA
[d] Department of Surgery, University of California Los Angeles, Los Angeles, CA, 90095, USA
[e] Department of Pharmacology-Medicinal/Biological Chemistry, University of Toledo College of Medicine and Life Sciences, Toledo, OH, 43614, USA
[f] Crump Institute for Molecular Imaging, University of California Los Angeles, Los Angeles, CA, 90095, USA
[g] Department of Molecular and Medical Pharmacology, University of California Los Angeles, Los Angeles, CA, 90095, USA
[h] Jonsson Comprehensive Cancer Center, University of California Los Angeles, Los Angeles, CA, 90095, USA

ARTICLE INFO

Keywords:
BIRC5
Gaussia luciferase
Pancreatic cancer
Super promoter
Thymidine kinase, microPET/CT imaging

ABSTRACT

Pancreatic ductal adenocarcinoma (PDAC) is a major cause of cancer mortality with a dismal overall survival rate and an urgent need for detection of minute tumors. Current diagnostic modalities have high sensitivity and specificity for larger tumors, but not for minute PDAC. In this study, we test the feasibility of a precision diagnostic platform for detecting and localizing minute human PDAC in mice. This platform includes: 1) defining BIRC5 as an early PDAC-upregulated gene and utilizing an enhanced BIRC5 super-promoter to drive expression of dual Gaussia luciferase (GLuc) and sr39 thymidine kinase (sr39TK) reporter genes exponentially and specifically in PDAC; 2) utilizing a genetically-engineered AAV_2^{RGD} to ensure targeted delivery of GLuc and sr39TK specifically to PDAC; 3) using serologic GLuc and sr39TK microPET/CT imaging to detect and localize minute human PDAC in mice. The study demonstrates feasibility of a precision diagnostic platform using an integrated technology through a multiple-stage amplification strategy of dual reporter genes to enhance the specificity and sensitivity of detection and localization of minute PDAC tumors and currently undetectable disease.

1. Introduction

Pancreatic ductal adenocarcinoma (PDAC) is the fourth leading cause of cancer mortality in the United States [1]. In 2017, there were 53,670 new cases and 43,090 deaths resulting from PDAC, which accounted for approximately 3% of all new cancer cases and 7% of all cancer deaths [1]. The estimated overall PDAC 5-year survival rate is 8%, and the 5-year survival in advanced stages is only 3% [1]. Early diagnosis significantly improves the survival of PDAC, the 5-year survival rate for patients with minute tumors smaller than 10 mm (TS1a) following surgery can reach 80–86% [2]. Therefore, a precision diagnostic platform for early detection and localization of minute PDAC tumors is urgently needed.

Pancreatic cancer is one of the most aggressive cancers. It is common for metastasis to have already occurred by the time a patient receives a diagnosis. However, metastases are frequently missed, and many patients with undetectable metastasis undergo surgery that does not provide significant survival benefit. On the other hand, benign pancreatic masses are often treated as minute PDAC tumors. Therefore, unnecessary surgeries are performed because traditional imaging techniques cannot discriminate minute PDAC tumors from benign pancreatic masses and cannot detect small metastases [3,4]. Noninvasive reporter gene imaging (NRGI) can provide noninvasive assessments of endogenous biologic processes in patients and can be performed using different imaging modalities [5], however, insufficient transgene expression and lack of tumor specificity limit clinically effective NRGI. Non-imaging based diagnostic modalities for PDAC have included circulating biomarkers based on “omics” analyses, such as proteins, nucleic acids, circulating tumor cells (CTCs), and exosomes, and are promising, but have not yet reached clinical applicability.

* Corresponding author. Department of Surgery, University of Toledo College of Medicine and Life Sciences, Toledo, OH, 43614, USA.
E-mail address: francis.brunicardi@utoledo.edu (F.C. Brunicardi).

https://doi.org/10.1016/j.canlet.2019.04.036
Received 13 February 2019; Received in revised form 25 April 2019; Accepted 29 April 2019

33–46% of patients treated with pancreatic surgery have undetectable metastases or benign pancreatic masses that do not justify surgical intervention. Therefore, a precision diagnostic platform that can differentiate minute resectable PDAC from currently undetectable metastases or benign masses is needed to improve survival for patients with resectable PDAC and avoid unnecessary surgical risk. One strategy for that is an integrated technology using a multiple-stage amplification strategy of dual reporter genes to enhance the specificity and sensitivity of detection and localization of minute PDAC tumors and currently undetectable disease. The sensitivity and specificity of this precision diagnostic platform was tested in ***in vitro*** **and** ***in vivo*** human PDAC models as a feasibility study.

2. Materials and methods

2.1. Cell lines, vectors, and antibodies

2.1.1. Cell lines

Human pancreatic cancer cell lines (PANC-1, Mia PaCa2, Capan2, and AsPc1) were purchased from the American Type Culture Collection (ATCC, Bethesda, MD) every 6 months. Human embryonic kidney cells, HEK 293FT, were purchased from ThermoFisher Scientific (ThermoFisher Scientific, MA). The cell lines were maintained in Dulbecco's modified Eagle medium (ThermoFisher Scientific, MA) supplemented with 100,000U/L of penicillin, 100,000μg/L of streptomycin, and 10% fetal bovine serum (FBS). Human primary pancreatic cells epithelial cells (HPPE) were purchased from Cell Biologics, Inc. (Chicago, IL). Human pancreatic ductal epithelial (HPDE) cell line was kindly provided by Ming-Sound Tsao (University of Toronto, Toronto, Ontario, Canada) and authenticated by short tandem repeat analysis (STR) using Promega kit with 16 STR loci every 6 months. Patient derived cell lines (PDCL-15, original name TKCC-15-Lo) was kindly provided by Dr. Andrew Biankin from Wolfson Wohl Cancer Research Centre, UK with authentication by STR. PDCL-15 was maintained in M199/F12 (Ham mixture) media mixed 1:1 with Ham's F-12 and supplemented with 15 mM HEPES, 1x MEM vitamin solution, 20 mM glutamine, 25 μg/mL human apo-transferrin, 20 ng/mL human recombinant EGF, 0.2IU/mL Insulin, 0.5 pg/mL Triiodothyronine, 40 ng/mL hydrocortisone, 2 μg/mL Ophosphorylethanolamine, 0.06% glucose solution, and 7.5% Fetal Calf Serum (FCS).

2.1.2. Vectors

AAVpro Helper Free System (AAV2) and AAVpro™ Extraction Solution were purchased from Clontech (Mountain View, CA). Human p53-(1–320) ($p53^{(1-320)}$) was a gift from Cheryl Arrowsmith (Addgene plasmid #24864). pBabe-Kras G12D was a gift from Channing Der (Addgene plasmid # 58902). AAV:ITR-U6-sgRNA(Kras)-U6-sgRNA(p53)-U6-sgRNA(Lkb1)-pEFS-Rluc-2A-Cre-shortPA-KrasG12D_HDRdonor-ITR (AAV-KPL)(Plasmid #60224), lentiGuide-Puro (Plasmid #52963), lentiCas9-Blast (Plasmid #52962), psPAX2 (plasmid #12260), and pMD2.G (plasmid #12259) were gifts from Feng Zhang (Addgene).

2.1.3. Antibodies

Anti-human and mouse $Kras^{G12D}$ (14429S) and human p53 (2527T) were purchased from Cell Signaling Technology (Danvers, MA). Anti-Integrin αVβ5, Alexa Fluor® 488 conjugated, anti-Heparin/Heparan Sulfate, Anti-Integrin αVβ3 Antibody, and Alexa Fluor®488 conjugated were purchased from Millipore (Billerica, Massachusetts). Anti-HSV-1 thymidine kinase (sc-28038), human HPA-1 (sc-25825), human anti-Smad4 (sc-7966) and anti-p15/p16 (sc-377412), and mouse anti-p53 (sc-6243) were bought from Santa Cruz (Dallas, TX). Anti-β-Actin antibody, anti-HA antibody, and anti-FLAG® M2 antibody were purchased from Sigma-Aldrich (St. Louis, MO). Anti-adeno-associated Virus, VP1, VP2, and VP3, antibodies were purchased from GeneTex Inc. (Irvine, CA). Human Survivin (ab76424), mouse Rabbit-Survivin (ab469), Anti-Rabbit IgG H&L (Cy3 ®) preadsorbed (ab6939), Anti-Rabbit IgG H&L (Alexa Fluor® 555) (ab150074), Anti-Mouse IgG H&L (Alexa Fluor® 488), Anti-Mouse IgG H&L (Alexa Fluor® 594), and Anti-Goat IgG H&L (Alexa Fluor® 488) (ab150129) were purchased from Abcam (Cambridge, MA).

2.2. Construction and preparation of lentiviral vectors

LentiCas9-tdtomato-blast (LentiCas9-tdT) was generated by ligation of Cas9 and tdTomoto through T2A peptide. A LentiGuide vector was generated by cloning GFP in pCDH-CMV-MCS-EF1-Neo (System Biosciences, Mountain View, CA) followed by insertion of a human $Kras^{G12D}$ homology directed repair (HDR) donor (for human) or a mouse HDR donor (for mouse). Gene-specific sgRNA oligos were cloned into the lentiGuide-Puro. The sgRNA sequences targeting $Kras^{G12D}$, TP53, P16, and SMAD4 were designed by the CRISPR Design Tool (http://crispr.mit.edu/) and synthesized by IDT. All the sgRNA sequences were listed. All constructs were sequence verified. Lentiviruses were produced by transfecting HEK 293T cells with the vector, pMD2.G and psPAX2 DNAs in 5:2:3 ratio with PEI. After 48 h of culturing, the viral supernatant was collected and passed through a 45 μm filter. Lentiviral particles were precipitated and concentrated with PEG-it by centrifugation at 1,500*g* for 30 min at 4 °C. The lentiviruses were re-suspended in 500 μl PBS and frozen in a −80 °C freezer.

2.3. Culture of human primary pancreatic ductal epithelial cells and murine organoids

2.3.1. Human primary pancreatic cells epithelial cells (HPPE)

Human primary pancreatic cells epithelial cells (HPPE) were purchased from Cell Biologics, Inc. (Chicago, IL) and grown in T25 tissue culture flasks pre-coated with gelatin-based coating solution for 2 min and incubated in *Cell Biologics'* Culture Complete Growth Medium (H6621, Cell Biologics Inc. IL). Human pancreatic ductal epithelial (HPDE) cell line was kindly provided by Ming-Sound Tsao (University of Toronto, Toronto, Ontario, Canada) and maintained in the keratinocyte-SFM supplemented with EGF and BPE (ThermoFisher Scientific, MA).

2.3.2. Culture of mouse pancreatic ductal organoids

Normal pancreatic ducts were harvested after enzymatic digestion of pancreas with 0.012% (w/v) collagenase XI (Sigma) and 0.012% (w/v) dispase II (Sigma) in DMEM media containing 1% FBS (Gibco). They were seeded in growth factor-reduced (GFR) Matrigel (BD) and cultured in human complete medium, as previously described [6]. In brief, the pancreatic tissue was minced and digested in digestion medium (DMEM supplemented with Penicillin/Streptomycin, 1% FBS, 0.012% (w/v) collagenase XI (Sigma) and 0.012% (w/v) dispase II) at 37 °C with continuous rotation for 20 min. The supernatant was transferred into a clean Petri dish. Pancreatic ducts were dissected and collected into the 15 ml tube and centrifuged at 140g for 5 min at 4 °C. After removal of supernatant, pancreatic ducts were suspended in Matrigel and seeded in 24-well plate. The remain pancreatic tissue were continuously digested and pancreatic ducts were collected after every 10 min incubation. The complete feeding medium (see supplemental data) was added into the 24-well plate where the Matrigel has been solidified after 20 min incubation at 37 °C.

2.4. CRISPR/Cas9 genomic editing with lentiviral infection

To introduce driver mutations in the HPPE cells, HPPE cells were co-infected with Lentiviral Cas9-tdT and Lentiviral-sgRNAs-$HDR^{KrasG12D}$-donors per protocol [7]. The sgRNA for human Kras mutation was designed to change the DNA code GGT that encoded glycine (G) at 12 to be aspartic acid (D) (sTable 1). The sgRNA for p53, p16 and SMAD4 were designed to induce indels at Q5 (glutamine 5) of P53, R51

(arginine 51) of p16 and Q284 (glutamine 284) of SMAD4. The sgRNA for murine organoid CRISPR/Cas9 engineering was following the published research design [8] Organoids were broken down into small cell clusters, which were re-suspended in 250 µl of 2 x feeding medium supplemented with 4 µg/ml of polybrene (Sigma-Aldrich, MO) followed by mixing with 250 µl of viral mixture and then transferred into a 48-well culture plate. The plate was centrifuged at 800 rpm at 32 °C for 60 min, followed by another 6 h of incubation at 37 °C. The cells were transferred into 1.5 ml Eppendorf tube and spun down at 800 rpm for 5 min. The supernatant was discarded, and the pellet was re-suspended in 100 µl Matrigel (BD Biosciences) and split into two wells of a 24-well culture plate. After solidification at 37 °C for 60 min, each well was overlaid with 500 µl of infection medium. Media were replaced twice a week, and spheres were collected after 2–3 weeks for passaging. Static images of spheres were collected using an Olympus fluorescence inverted microscope (Olympus, Japan).

2.5. AAV vector particle production

AAV-targeting vectors and AAV_2 were generated using the AAVpro™ Helper Free System (AAV_2) (Clontech, Mountain View, CA). For production of the targeting vectors, pRC2-mi342 was engineered by insertion of tumor homing peptide sequence. $pAAV_2$-CMV vectors were engineered to generate $pAAV_2$-CMV-GLuc, $pAAV_2$-CMV-eGFP, $pAAV_2$-CMV-FLuc, $pAAV_2$-BIRC5-SP^{TSTA}-GLuc-2A-sr39TK vectors and $pAAV_2^{RGD}$-BIRC5-SP^{TSTA}-GLuc-2A-sr39TK vectors. AAV_2^{RGD}-BIRC5-SP^{TSTA}-GLuc-2A-sr39TK vector is a highly-specific PDAC viral vector that has been engineered to display RGD peptide on its surface aimed to attach to PDAC cells to deliver GLuc and sr39TK genes into PDAC specifically. Whereas GLuc and sr39TK genes are linked by 2A sequence and controlled by TSTA-enhanced BIRC5 super-promoter, which are therefore only expressed in PDAC cells. GLuc-2A-srTK39 proteins are then into GLuc and srTK39 reporters in PDAC cells.

For production of AAV_2 wild-type (AAV_2^{WT}) and AAV_2 genetically engineered (AAV_2^{GE}), HEK-293FT cells were transfected with plasmids $pAAV_2$, pRC2-mi342, and pHelper vector in an equal molar ratio mixed with PEI. Cells were harvested, pelleted by centrifugation, and lysed post 48 h of transfection. Cell lysates were treated with 50 U/ml Benzonase (Sigma-Aldrich,) at 30 min, 37 °C. Lysates (3,500 *g*, 20 min, 4 °C) were purified by iodixanol gradient purification for 2 h at 290,000 g in a Beckman 70Ti rotor and harvested from the 40% iodixanol layer.

2.6. Optical imaging and serum GLuc measurement

Animal experiments were performed in accordance with IACUC guidelines. Ten to 8-week-old male Nude/Nude mice (Charles River Laboratories, Inc. Wilmington, MA) were subcutaneously implanted with 1×10^6 Mia PaCa2 or Capan2 cells stably expressing GLuc-2A-sr39TK with Matrigel. Optical imaging was performed with an IVIS CCD camera (IVIS Lumina II, Perkin Elmer, Waltham, MA) on day 8, 14, 21, and 30. Mice were anesthetized with isoflurane, and then given 100 µg/50 µl of water-soluble coelenterazine per mouse (Nanolight Technology, Pinetop, AZ) *via* tail vein and immediately imaged and analyzed using the Living Image Software (Caliper Life Sciences). For measurement of serum GLuc levels, 50 µl blood per mouse were collected from xenograft tumor mice *via* tail vein on days 2, 4, 7, 14, 21, and 30 after cancer cell implantation and serum was extracted; 50 µl serum was used for evaluation of GLuc levels.

2.7. MicroPET/CT imaging

Engineered patient-derived PDAC cell line-15 (PDCL-$15^{CMV-GLuc-2A\text{-}sr39TK}$) cells versus control PDCL-15^{WT} cells were implanted in the right and left flanks, respectively, of the same mouse. On day 8, tumors reached 10 mm, defined as a minute human PDAC tumor, animals were optically imaged followed by injection with 200 µCi [^{18}F] FHBG *via* the tail vein. Following an hour of substrate uptake, the entire animal was scanned for 20 min in a micro-PET/CT scanner (Genisys, Sofie Biosciences, CA), and imaged for 15 min at 50 keV, 325 µA, and 196 total angles of rotation in two bed positions. After 24 h, mice were injected with 200 µCi [^{18}F]FDG *via* the tail vein, and micro-PET/CT scanning was performed. All microPET/CT data analyses and 3-D images were compiled using AMIDE.

2.8. Targeting AAV_2 detection virus delivery and tumor imaging

Ten 6 to 8-week-old nude mice were engrafted subcutaneously with 1×10^6 PANC-1 tumor cells. When tumors reached 4.5 mm, defined as a minute human PDAC tumor, 8×10^{11} genome copies (gc) of AAV_2^{WT}-CMV-GLuc-2A-sr39TK, AAV_2^{RGD}-CMV-GLuc-2A-sr39TK or AAV_2^{RGD}-BIRC5-SP^{TSTA}-GLuc-2A-sr39TK were injected *via* tail vein and luciferase signals were detected by optical imaging 1-week post-injection.

2.9. Statistical analysis

Data from western blot, reporter assays, and immunohistochemistry experiments were analyzed by two-tailed *t*-test in Excel. All error bars indicate s.d. unless stated otherwise. Organoid size and shape measurements were analyzed by *t*-test using GraphPad Prism. One-way ANOVA was used to compare and correlate multiple groups using GraphPad Prism 6.

3. Results

3.1. AAV_2^{RGD}-BIRC5-SP^{TSTA}-GLuc-2A-sr39TK is highly efficient and specific for detection and localization of minute human PDAC tumors in mice

AAV_2^{RGD}-BIRC5-SP^{TSTA}-GLuc-2A-sr39TK vector is a viral vector that is highly specific for PDAC, as the engineered viral surface RGD specifically binds to integrin on PDAC cell surface and the TSTA enhanced BIRC5 super promoter is only activated in the PDAC cells. In addition, enhanced super-promoter contributes to highly sensitive detection of BIRC5 expression. To evaluate the sensitivity and specificity of AAV_2^{RGD}-BIRC5-SP^{TSTA}-GLuc-2A-sr39TK to detect minute PDAC tumors in xenograft mice, 1×10^6 PANC1 cells were implanted into the flank of nude mice and allowed to grow for two weeks to a size of 4.5 mm, defined as a minute human PDAC tumor. Control mice were non-tumor bearing. PANC-1 cells were chosen, as they express BIRC5 and integrin and harbor $Kras^{G12D}$ and $p53^{R273H}$ mutations. AAV_2^{RGD}-BIRC5-SP^{TSTA}-GLuc-2A-sr39TK (versus control vectors AAV_2^{RGD}-CMV-GLuc-2A-sr39TK or AAV_2^{WT}-CMV-GLuc-2A-sr39TK) was systemically administrated *via* tail vein injection (2×10^{11} vp; n = 10/group; 5 males; 5 females). Imaging studies and serologic GLuc levels were performed at 1 week; no toxicity was observed in any group. AAV_2^{RGD}-BIRC5-SP^{TSTA}-GLuc-2A-sr39TK resulted in a strong signal from a 4.5 mm PANC-1 tumor with complete absence of non-specific signals (Fig. 1 A1; red circle). Control AAV_2^{RGD}-CMV-GLuc-2A-sr39TK resulted in significantly less tumor signaling with extensive non-specific signaling (Fig. 1 A2; red circle). Control vector AAV_2^{WT}-CMV-GLuc-2A-sr39TK resulted in negligible tumor signaling with extensive, diffuse and non-specific signals (Fig. 1 A3; yellow circle). Correspondingly, quantification of bioluminescence images revealed high, low, and minimal photon levels for tumor imaging, respectively (Fig. 1 B1, B2 and B3), as well as absent, moderate and high levels of photons for background signals in mice given AAV_2^{RGD}-BIRC5-SP^{TSTA}-GLuc-2A-sr39TK, AAV_2^{RGD}-CMV-GLuc-2A-sr39TK, or AAV_2^{WT}-CMV-GLuc-2A-sr39TK, respectively (Fig. 1 C1, C2 and C3). There was high correlation of the images with serologic GLuc levels in AAV_2^{RGD}-BIRC5-SP^{TSTA}-GLuc-2A-sr39TK, resulting in high serum GLuc levels in PDAC tumor bearing mice (Fig. 1 D1; black bar) and no levels seen in non-tumor mice (Fig. 1 D1; white

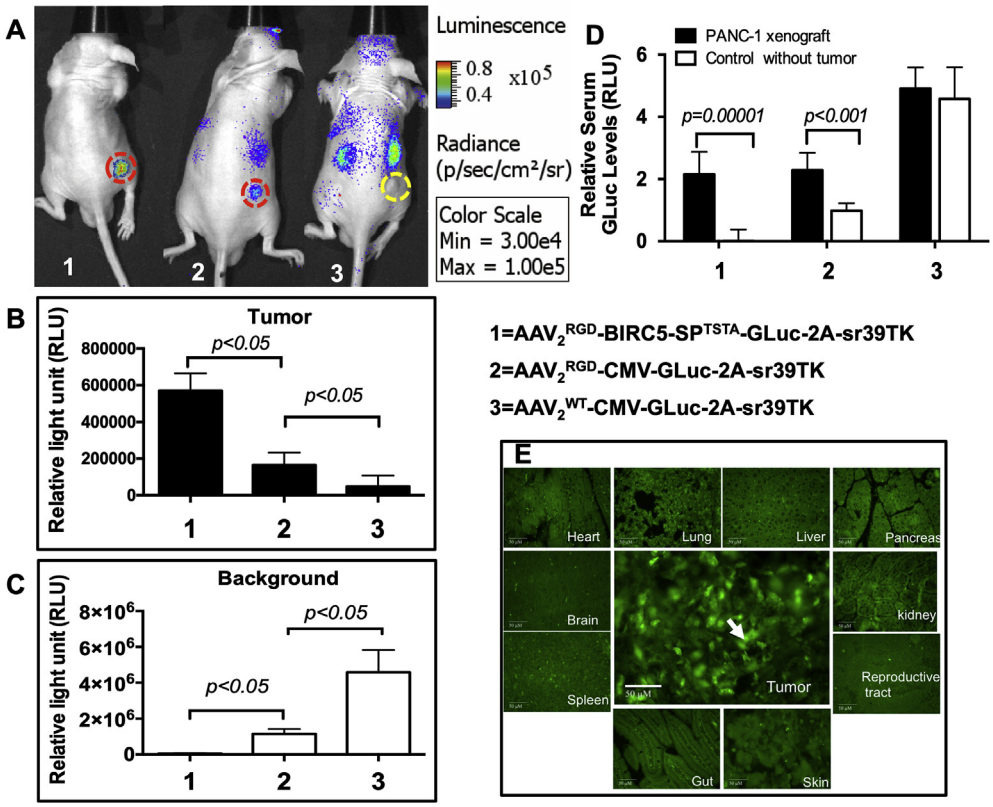

Fig. 1. Feasibility of the precision diagnostic platform is demonstrated using systemic delivery of 1) AAV_2^{RGD}-BIRC5-SP^{TSTA}-GLuc-2A-sr39TK (1), 2) control AAV_2^{RGD}-CMV-GLuc-2A-sr39TK (2) or 3) control AAV_2^{WT}-CMV-GLuc-2A-sr39TK (3) into xenograft PANC1 tumor model. Bioluminescence imaging of xenograft mouse model using systemic delivery of AAV_2^{RGD}-BIRC5-SP^{TSTA}-GLuc-2A-sr39TK demonstrated a highly specific PDAC tumor signal (A1; red circle) with no background noise, which were quantified in B1 and C1, respectively. Systemic delivery of control AAV_2^{RGD}-CMV-SP^{TSTA}-GLuc-2A-sr39TK demonstrated significantly less PDAC tumor signal (A2; red circle) with significantly greater non-specific background noise, quantified in B2 and C2, respectively. Systemic delivery of control AAV_2-CMV-SP^{TSTA}-GLuc-2A-sr39TK demonstrated minimal tumor signal (A3; yellow circle) with even greater non-specific background noise, quantified in B3 and C3, respectively. Imaging data of AAV_2^{RGD}-BIRC5-SP^{TSTA}-GLuc-2A-sr39TK highly correlated with serologic GLuc levels (D1; black bar) vs absence of GLuc in control mice without tumor (D1; white bar). Imaging data of both control vectors did not correlate with serologic GLuc levels (D2 and D3; black bars); nonspecific GLuc levels were found in control mice without tumors (D2 and D3; white bar). Immunofluorescence of tumors and benign tissues following systemic delivery of AAV_2^{RGD}-BIRC5-SP^{TSTA}-GLuc-2A-sr39TK demonstrated viral thymidine kinase (vTK) was highly expressed only in PDAC tumors, but not in benign tissues (E). (For interpretation of the references to color in this figure legend, the reader is referred to the Web version of this article.)

bar). Both control vectors resulted in serologic GLuc levels in both tumor bearing (Fig. 1 D2; black bar; D3; black bar) and non-tumor bearing mice (Fig. 1 D2; white bar; D3; white bar), demonstrating the lack of specificity to detect expression of GLuc in PDAC versus benign tissues in mice. Mice were sacrificed and necropsy was performed; tumors were excised and viral thymidine kinase (vTK) expression was measured in tumors and benign tissues. AAV_2^{RGD}-BIRC5-SP^{TSTA}-GLuc-2A-sr39TK resulted in high expression of sr39TK with no expression in benign tissues (Fig. 1, E). These data demonstrate the feasibility of a precision diagnostic platform utilizing AAV_2^{RGD}-BIRC5-SP^{TSTA}-GLuc-2A-sr39TK to sensitively and specifically detect and localize minute human PDAC tumors in mice.

3.2. Selection of BIRC5 as a prototype target gene of PDAC in vitro

Studies, including our own, have shown that BIRC5 is overexpressed in the majority of PDAC [9–11]. Therefore, we selected BIRC5 as the prototype PDAC-upregulated gene for the platform.

To investigate BIRC5 expression in engineered models of PDAC, $Kras^{G12D}$ or/and truncated P53 were over-expressed in benign human primary pancreatic ductal epithelial (HPPE) cells. Western blot analysis showed that BIRC5 expression was initiated in HPPE cells expressing $Kras^{G12D}$ and was augmented in HPPE expressing $Kras^{G12D}$/truncated p53 ($p53^{(1-320)}$) (Fig. 2A and B). Driver mutations, $Kras^{G12D}$, p53 deletion ($p53^{Del}$), $p16^{Del}$, and $SMAD4^{Del}$ were introduced into HPPE cells using CRISPR/Cas9. Co-transfection with sgRNAs and Cas9 was indicated by the presence of green and red colors in HPPE cells, respectively (Fig. 2C); cells were further sorted and enriched by flow cytometry (Fig. 2D). Mutations were confirmed by Sanger sequencing, colony PCR assays (sTable 1) and analyzed using CRISPR-ID web based software [12]. 37/40 $Kras^{G12D}$ (S1 A, B), 37/40 of $p53^{Del}$ (S1 C), 31/40 of $p16^{Del}$ (S1 D) and 34/40 of $SMAD4^{Del}$ colonies (S1 E) were successfully mutated. Upregulation of BIRC5 was evaluated using western blot analysis (Fig. 2E). $Kras^{G12D}$ alone resulted in low level BIRC5 expression in engineered HPPE cells, with a robust increase in BIRC5 expression following the addition of $p53^{Del}$ mutation (Fig. 2E). However, there were no further increases in BIRC5 expression following the addition of $p16^{Del}$ and $SMAD4^{Del}$ (Fig. 2E). Therefore, we chose to focus on $Kras^{G12D}$ and $p53^{Del}$ mutations for the following studies.

The time course for growth of state-of-the-art mouse 3D pancreatic ductal organoids with and without $Kras^{G12D}$ and $p53^{Del}$ driver mutations was captured using time-lapse video (IncuCyte S3, Essen Bioscience, Ann Arbor, Michigan) (Movie S1, S2). Co-transfection of lenti-gRNA (green) and lenti-Cas9tdt (red) was indicated within the organoids (Fig. 2F). Transformed organoids had tumor-like growth patterns (Fig. 2G, upper panel) with sgRNAs and $Kras^{G12D}$-HDR (GFP) and Cas9 (tdTomato), whereas wild-type organoids exhibited a circular pattern (Fig. 2G, bottom panel). Transformed organoids were observed within 5 days and displayed early PDAC morphology (Fig. 2F). Transformed organoid cross-sectional H&E staining, confirmed by 3 independent pathologists, was consistent with PDAC morphology, whereas that of wild-type organoids resembled normal ductal structures. Therefore, CRISPR/Cas9 engineering of pancreatic ductal organoids with driver mutations provides an excellent *in vitro* model to recapitulate development of minute PDAC.

Supplementary video related to this article can be found at https://doi.org/10.1016/j.canlet.2019.04.036.

Immunohistochemistry and western blot analyses were performed on transformed versus wild-type organoids on day 10 after infection (Fig. 2F). Expression of $Kras^{G12D}$ and deletion of P53 in transformed organoids were associated with BIRC5 upregulation (Fig. 2H, upper panel), whereas absence of $Kras^{G12D}$ and expression of wild type P53 in wild-type organoids was associated with complete absence of BIRC5 expression (Fig. 2H, bottom panel). These data demonstrate that BIRC5

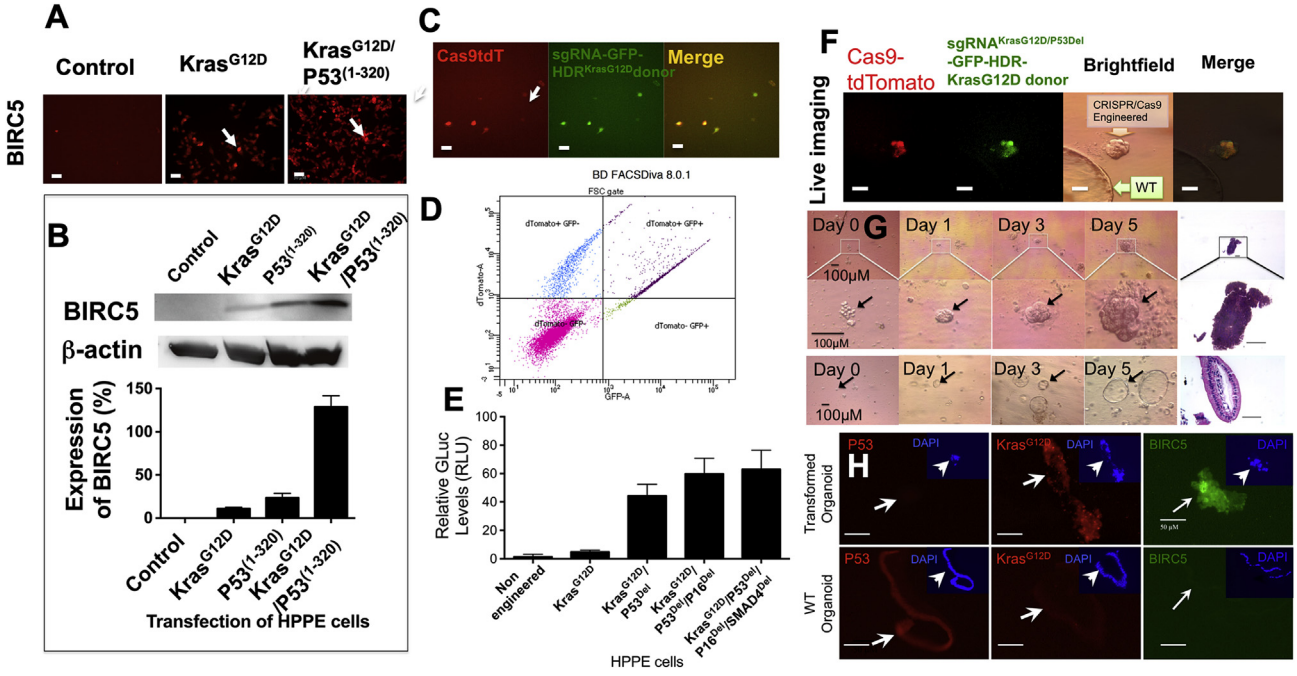

Fig. 2. BIRC5 was selected as the prototype for PDAC overexpressed gene. Initiation of expression of BIRC5 was triggered by overexpression of $Kras^{G12D}$ or $P53^{(1-320)}$ (expression of 1–320 amino acid of P53) in benign human primary pancreatic epithelial cells (HPPE) and significantly increased by overexpression of $Kras^{G12D}$ and $P53^{(1-320}$ as shown in immunostaining (A) and western blot analysis (B). The pattern of expression of BIRC5 was further confirmed by CRISPR/Cas9 engineered HPPE cells and mouse pancreatic ductal organoids (ORGs). Driver mutation $Kras^{G12D}/p53^{Del}$ engineered HPPE cells were obtained by co-transfection with both gRNA (green) and Cas9 (red) (C) and enriched by flowtometry (D). The expression profiling of BIRC5 in driver mutation-engineered HPPE cells was determined by western blot (E). Successful infection of ORGs with lentiviral Cas9 (red) and gRNA (green) (F) resulted in transformation of organoids (G upper 2 panels) compared to wild-type organoids morphologically (G bottom panel). Absence of expression of p53 and over-expression of $Kras^{G12D}$ in transformed organoids resulted in over expression of BIRC5, as shown in the immunofluorescence staining (H upper panel); wild-type organoids expressing p53 and an absence of $Kras^{G12D}$ had no expression of BIRC5 (H bottom panel) (scale bar = 50 μm). (For interpretation of the references to color in this figure legend, the reader is referred to the Web version of this article.)

upregulation in PDAC reflects activation of common PDAC driver mutations and support our selection of BIRC5 as a prototype PDAC-upregulated gene.

3.3. BIRC5 super-promoter enhances gene expression in PDAC cells

Utilizing our technique of engineering synthetic promoters of overexpressed genes to target PDAC, a BIRC5 super-promoter (BIRC5-SP) was generated based on the analysis of key cis- and trans-regulatory elements located in the endogenous BIRC5 promoter between −327 and −1 (ATP), which were randomly repeated [13]. The elements of the promoter included the binding sites for EGR-1 (Early growth response protein 1), NF-kB, KLF5, STAT3, P53, E2F/RB, SP1, the CDE (Cell Cycle-dependent Elements) and CHR (Cell Cycle Genes Homology Region) (Fig. 3A) [14]. Fourteen BIRC5 synthetic promoter sequences were cloned into firefly luciferase reporter vector (S2-4) and screened in PDAC cells versus benign human pancreatic ductal cells (HPDE) and HPPE cells using a bioluminescent reporter assay (S5). The one with greatest promoter activity in PDAC cells and lowest activity in benign cells was defined as BIRC5-SP for further studies (S5); BIRC5-SP_S2; red arrows). BIRC5-SP drove GLuc expression with 15, 9, 13, and 6-fold higher activity compared to BIRC5-endogenous promoter (BIRC5-EP) in PANC-1, Mia PaCa2, Capan2, and AsPC-1 cells, respectively ($p < 0.05$) (Fig. 3B); no activity was observed in benign HPPE and HPDE cells due to absence of BIRC5 expression in these benign cells ($p > 0.05$). Furthermore, BIRC5-SP's activity was further enhanced by a two-step transcriptional amplification (TSTA) system (S6) [15]. TSTA significantly enhanced BIRC5-SP's activity up to 10-fold in BIRC5-SP^{TSTA} transfected PDAC and PDAC patient-derived cell lines, which express BIRC5, with no significant activity in benign HPDE cells, which do not express BIRC5 (Fig. 3C). Enhanced BIRC5-SP^{TSTA} activity was further validated using a GFP reporter (S7). The brightest signals were observed in the BIRC5-SP^{TSTA}-GFP transfected PDAC cells, whereas no signals were observed in benign HPPE cells. BIRC5-SP^{TSTA}-GLuc was further tested in transformed HPPE cells using BIRC5-SP-GLuc and CMV-GLuc as controls. BIRC5-SP^{TSTA}-GLuc resulted in significantly greater secreted GLuc levels compared to BIRC5-SP-GLuc and CMV-GLuc in both $HPPE^{KrasG12D}$ and $HPPE^{KrasG12D/P53Del}$ cells (Fig. 3D). Both BIRC5-SP^{TSTA}-GLuc and BIRC5-SP-GLuc resulted in no expression of GLuc in benign HPPE cells, whereas CMV-GLuc resulted in high expression of GLuc in wild-type HPPE cells (Fig. 3D). Lentiviral vector BIRC5-SP^{TSTA}-GLuc was selected to infect transformed versus wild-type mouse pancreatic ductal organoids (ORGs), resulting in secreted GLuc sensitively detected in transformed ORGs, but not wild ORGs. Higher GLuc levels were measured in medium of $ORG^{KrasG12D/P53Del}$ versus that of $ORG^{KrasG12D}$ (Fig. 3E). GLuc levels in transformed ORGs were highly correlative with BIRC5 expression, as determined by Western blot ($R = 0.97$) (Fig. 3F and G). Therefore, the assay using the enhanced BIRC5-SP^{TSTA} to drive the secreted reporter, GLuc, was highly sensitive and specific in reflecting BIRC5 expression levels in transformed organoids and PDAC cells *in vitro*.

3.4. Dual reporter genes: serologic and optical imaging Gaussia luciferase and sr39TK microPET/CT imaging reporters can detect and localize minute PDAC

To test the sensitivity of GLuc assay, stably transfected Mia $PaCa2^{CMV-GLuc}$ and $Capan2^{CMV-GLuc}$ cells were studied. 100 PDAC cells/ml of culture medium produced detectable levels of secreted GLuc and the signal increased proportionally with cell growth (Fig. 4A), suggesting remarkable sensitivity *in vitro*. To demonstrate that GLuc-2A-sr39TK could serve a dual-diagnostic role for both detection and

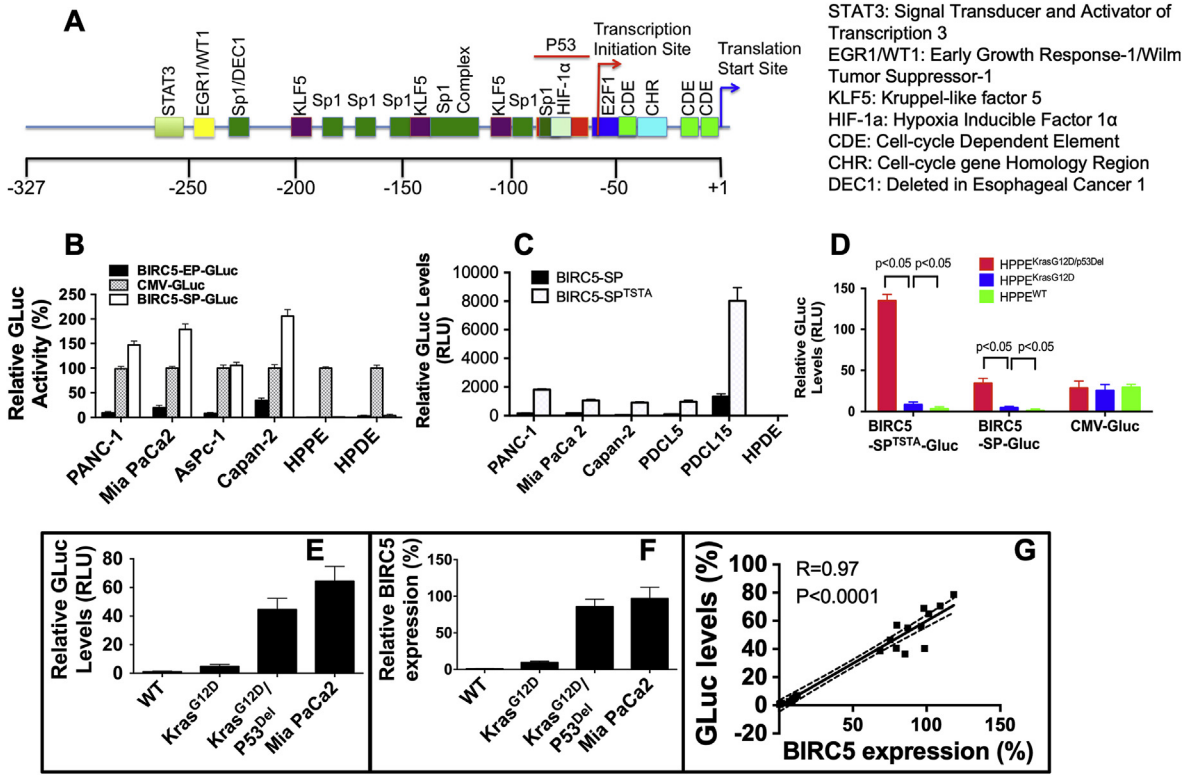

Fig. 3. Generation of BIRC5 super-promoter. BIRC5 synthetic promoters were designed based on the regulatory elements of proximate BIRC5 endogenous promoter (A). The BIRC5-SP was validated using the GLuc assay and demonstrated markedly increased expression of GLuc compared to BIRC5-EP in PDAC cell lines with no expression seen in benign pancreatic cell lines (B). BIRC5-SP activity was further enhanced using two-step transcriptional amplification (BIRC5-SP^{TSTA}), which resulted in 10-fold higher promoter activity than that of BIRC5-SP in PDAC cells, and no significant expression in benign HPPE cells (C). Transient transfection of HPPE^{KrasG12D}, HPPE$^{KrasG12D/P53Del}$ and benign HPPE^{WT} cells with BIRC5-SP^{TSTA}-GLuc, BIRC5-SP-GLuc and CMV-GLuc revealed that BIRC5-SP^{TSTA}-GLuc resulted in significantly greater secreted GLuc levels and specifically in both HPPE^{KrasG12D} and HPPE$^{KrasG12D/P53Del}$ cells compared to BIRC5-SP-GLuc and CMV-GLuc (D). Wild-type and transformed organoids were infected by lentivirus BIRC5-SP^{TSTA}-GLuc. GLuc culture media levels and BIRC5 expression levels were determined by bioluminescence assay western blot, respectively. Secreted GLuc levels (E) and BIRC5 expression levels (F) were each progressively higher in ORG^{KrasG12D}, ORG$^{KrasG12D/P53Del}$, and MIA PaCa2 (positive controls), which were highly correlated (R = 0.97) (G). No secreted GLuc or expression of BIRC5 was observed in WT ORGs (E, F and G). Therefore, BIRC5-SP^{TSTA}-driven GLuc secretion is a highly sensitive assay of BIRC5 expression in PDAC cell lines.

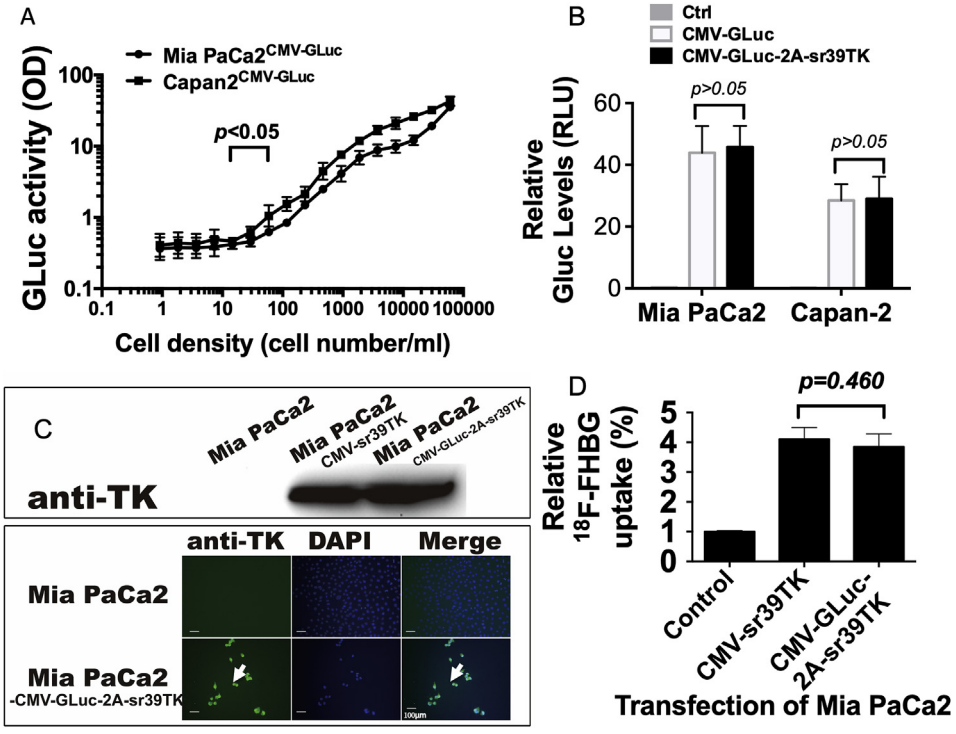

Fig. 4. Evaluation of activities of GLuc and sr39TK in GLuc-2A-sr39TK transfected cells. GLuc levels in cell culture medium of Mia PaCa2 and Capan-2 cells expressing GLuc demonstrates that 100 cells in one ml medium can be detected, thus GLuc is a highly sensitive serologic reporter (A). To determine if dual reporter Gluc-2A-sr39TK affects GLuc secretion or sr39TK's activity, transfection of Mia PaCa2 and Capan-2 cells with CMV-GLuc-2A-sr39TK versus CMV-GLuc or CMV-sr39TK was performed. Gluc-2A-sr39TK neither reduced the secretion of GLuc in Mia PaCa2 and Capan-2 cells (B), nor affected TK's expression (C) and activity (D) in Mia PaCa2 cells, as determined by immunofluorescence assay (scale bar = 100 μm) and ^{18}F-FHBG uptake assay, respectively. These *in vitro* data support the hypothesis that GLuc-2A-sr39TK can be used as dual diagnostic reporters to detect and localize PDAC.

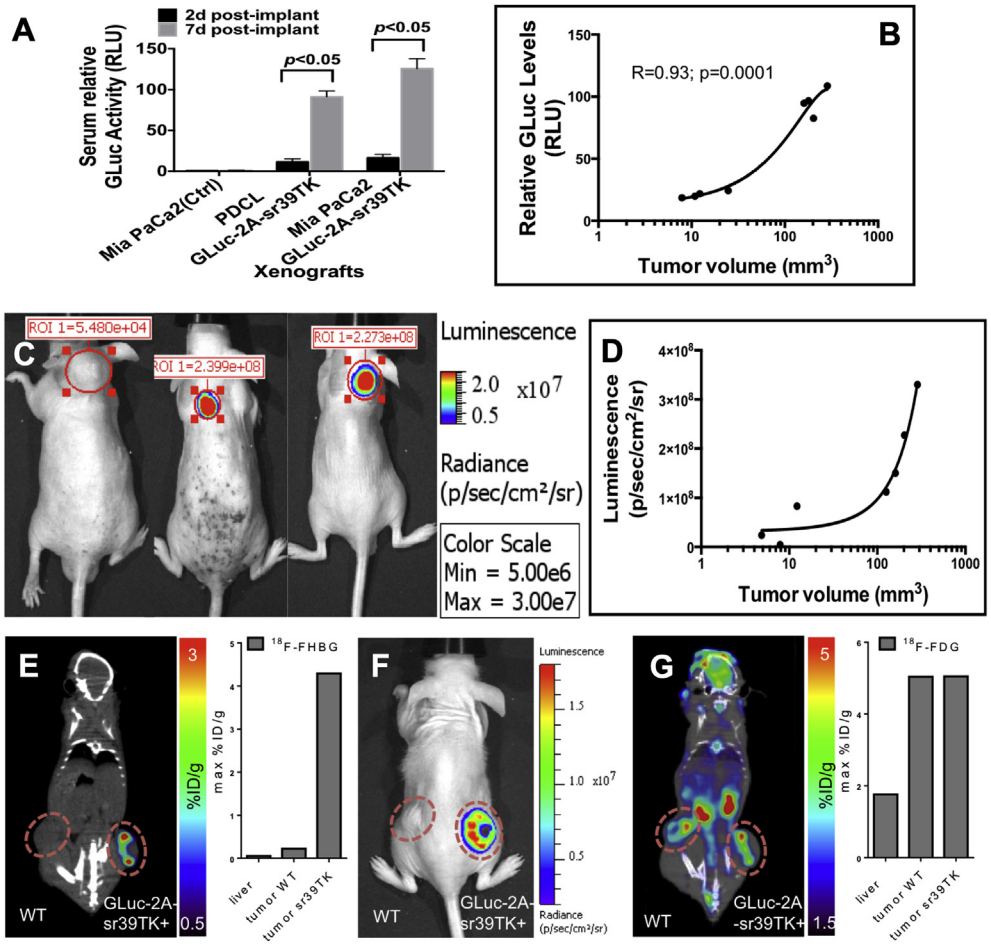

Fig. 5. Xenograft tumor models were generated by subcutaneous injection of Mia PaCa2 or patient-derived PDAC cell line (PDCL-15), both stably expressing GLuc-2A-sr39TK. 50ul of blood were collected on day 2 and 7 after inoculation of PDAC cells. Serum GLuc levels increased with tumor growth (A) and correlation between serum GLuc levels and minute tumor volume was highly significant (B; R = 0.93, p = 0.001). Optical imaging of PDAC tumors demonstrated strong signals in PDCL-15 and Mia PaCa2 tumors expressing GLuc-2A-sr39TK and no signal in control tumors (C) with a highly significant correlation of tumor volume and bioluminescence emitted photons (D; R = 0.92; p = 0.0005). In a second study, PDCL-15 cells stably expressing GLuc-2A-sr39TK were implanted in the right flank and control patient derived PDAC cells (PDCL-15) were implanted in the left flank. In two weeks, [^{18}F]FHBG microPET/CT was performed and demonstrated highly specific imaging of the minute PDCL-15 tumor with no imaging of the control cells and no background noise (E; orange circles), which correlated to bioluminescence imaging with coelenterazine, (F; orange circles). However, standard [^{18}F]FDG microPET/CT imaging revealed non-specific imaging of the both PDCL-15 tumors expressing GLuc-2A-sr39TK and control PDCL-15 tumors with extensive non-specific background noise (G; orange circles). These data demonstrate that GLuc-2A-sr39TK is highly sensitive and specific to localize minute PDAC tumors using microPET/CT imaging, and support the hypothesis that GLuc-2A-sr39TK can be used as a precision diagnostic platform for minute human PDAC. (For interpretation of the references to color in this figure legend, the reader is referred to the Web version of this article.)

localization of PDAC, we performed transient transfection of PDAC cells with a CMV-driven GLuc-2A-sr39TK vector, which resulted in similar levels of secreted GLuc to that of CMV-GLuc (Fig. 4B) and equivalent expression of sr39TK to that of CMV-sr39TK (Fig. 4C). sr39TK activity was not affected by the expression of GLuc-2A-sr39T (Fig. 4D). These data demonstrate effective cleavage and separate expression of GLuc and sr39TK *in vitro*.

Human PDAC xenograft mouse models were generated using engineered patient-derived PDAC cell line-15, (PDCL-15$^{CMV-GLuc-2A-sr39TK}$), Mia PaCa2$^{CMV-GLuc-2A-sr39TK}$, or non-transfected Mia PaCa2 cells (6 mice/group: 3 males/3 females). Serologic GLuc levels were detected at 10 mm^3 (1 mm diameter) PDAC tumor volume, whereas GLuc levels were undetectable in control mice (Fig. 5A). Rising serologic GLuc levels highly correlated with increasing PDAC tumor volume (Fig. 5B). GLuc bioluminescent imaging signals were highly proportional to tumor volume (R = 0.92; p = 0.005) (Fig. 5C and D). These data demonstrated remarkable sensitivity of serologic and optical imaging GLuc for detection and localization of minute human PDAC *in vivo*.

To evaluate microPET/CT imaging of human PDAC tumors, PDCL-15$^{CMV-GLuc-2A-sr39TK}$ cells versus control PDCL-15^{WT} cells were implanted in the right and left flanks, respectively, of the same mouse. When tumors reached 10 mm diameter, defined as a minute human PDAC tumor, mice underwent [^{18}F]FHBG microPET/CT (PDAC-specific imaging) and [^{18}F]FDG microPET/CT imaging (standard, non-specific imaging), as well as bioluminescence imaging. Three hours after injection of the specific TK probe, [^{18}F]FHBG, microPET/CT revealed highly specific imaging of minute PDAC tumors only in the right flank (Fig. 5E), which was consistent with results seen with bioluminescence imaging following injection of coelenterazine (Fig. 5F). Conversely, injection of [^{18}F]FDG microPET/CT, resulted in non-specific signals seen in both tumors and normal tissues (Fig. 5G). Therefore, expression of GLuc-2A-sr39TK in human PDAC tumors was sensitively and specifically detected by microPET/CT imaging, which correlated with optical imaging. These data support the hypothesis that PDAC expressing dual reporter genes could be used to detect and localize minute human PDAC tumors in mice using serologic and optical imaging GLuc and sr39TK/microPET/CT imaging, respectively.

3.5. Genetically-engineered recombinant adeno-associated virus 2 (AAV_2^{RGD}) enhances specific gene delivery in PDAC

AAV_2 was chosen as the delivery system due to its high gene delivery efficiency and proven safety in clinical trials [16,17]. AAV2 uses cell surface heparan sulfate (HS), a highly sulfated polysaccharide, as a receptor to establish infections. However, PDAC cells lose HS expression on their surface due to high levels of heparinase-1 (HPA-1) expression (S8), which results in low infection by wild type AAV_2. Therefore, we engineered the fundamental cellular attachment receptor of AAV_2, heparin sulfate proteoglycan (HSPG), with tumor homing peptides (TumorHoPe) on the viral capsid R588 site to enhance gene delivery specifically to PDAC (S9). Eighteen TumorHoPe sequences were selected from the TumorHoPe database (http://crdd.osdd.net/raghava/tumorhope/) (sTable2), which contains 744 entries of experimentally characterized TumorHoPe. Capsid mutations at R585A and R588A served as controls. PDAC-specific AAV_2 viruses were

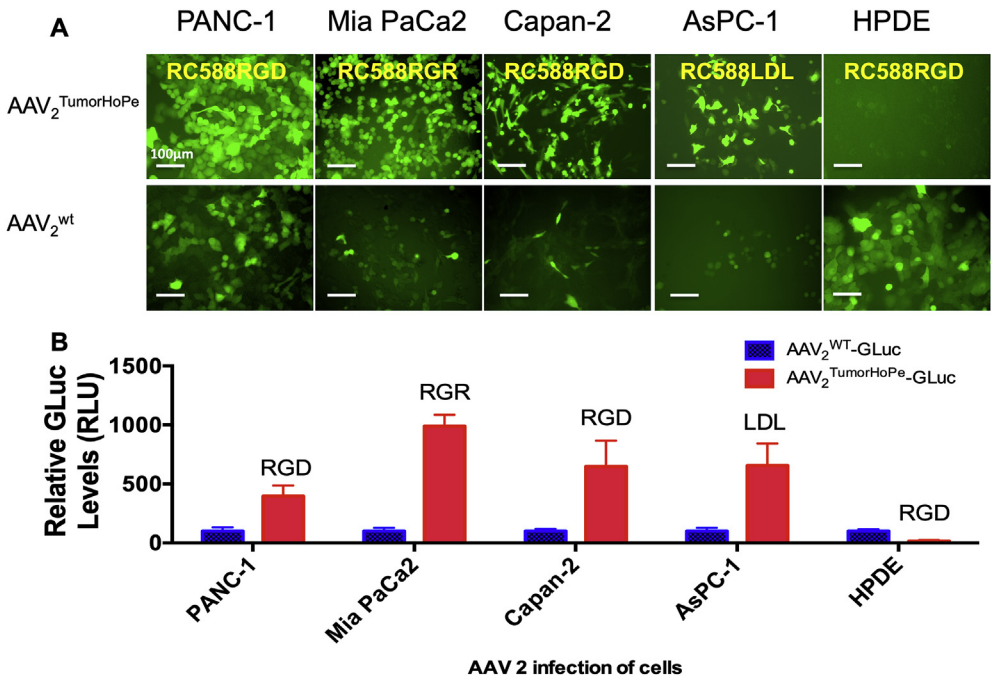

Fig. 6. Using a screening assay, five tumor homing peptide-engineered AAV_2 viruses ($AAV_2^{TumorHoPe}$) with the highest infectivity were selected for validation in PDAC cells. GFP assay demonstrated that $AAV_2^{TumorHoPe}$ enhanced viral infectivity specifically in PDAC cells, but not in benign HPDE cells (6A; top panel). AAV_2^{WT} had far less viral infectivity in PDAC cells, and marked infectivity in benign HPDE cells (6A; bottom panel) (scale bar = 100 μm). GLuc reporter assay demonstrated that $AAV_2^{TumorHoPe}$ enhanced viral infectivity specifically in PDAC cells, but not in benign HPDE cells (6B; red bars). AAV_2^{WT} had significantly less viral infectivity in PDAC cells, and equivalent infectivity in benign HPDE cells (6B; blue bars). The data demonstrate high specificity of $AAV_2^{TumorHoPe}$ for PDAC delivery of reporter genes. (For interpretation of the references to color in this figure legend, the reader is referred to the Web version of this article.)

identified using a CMV-driven firefly luciferase (CMV-FLuc) reporter assay in PDAC cell lines versus benign HPDE and HPPE cells (S10). Optimal vectors in each cell line were selected based upon the highest infection rate of PDAC cells and the lowest infection rate of benign human pancreatic cells. AAV_2^{RGD} optimized targeting in PANC-1, Capan2, AsPC1 with no activity in benign HPDE and HPPE cells, therefore these engineered viruses were selected for further validation using GFP and GLuc reporter assays in PDAC cells. GFP expression (Fig. 6A) and GLuc expression (Fig. 6B) in each matched cell line were consistent with the findings of the FLuc reporter assay (S13). To further determine whether the specificity of infection was dependent upon specific ligand receptor binding, a competition assay was performed and revealed that high dose peptides inhibited infection of each cell by its corresponding virus (S11). Since integrin was highly expressed in the PDAC cells, but not benign human pancreatic cells (S12) [18], AAV_2^{RGD} was selected as the delivery system and was shown to be highly specific for PDAC cell delivery as seen in Fig. 1.

4. Discussion

In this feasibility study, a precision diagnostic platform was developed to detect and localize minute human PDAC tumors in mice using an enhanced BIRC5 super-promoter to drive two reporter genes, delivered by an engineered PDAC-specific adeno-associated virus. BIRC5, the gene that codes for the anti-apoptosis protein Survivin, has been defined as a target in many cancers, including PDAC, and was chosen as the prototype PDAC over-expressed gene [11]. BIRC5 is prominently expressed during embryonal development, is absent in most terminally differentiated tissues, and upregulated in a variety of human cancers [19]. It is over-expressed in 77–94% of PDAC, including pre-invasive PanIN3 and metastatic PDAC, but is absent in benign pancreatic tissue [9–11]. The organoid model and cell lines in this study revealed that BIRC5 is upregulated in the presence of Kras mutation and further augmented with P53 deletion confirming that common PDAC Kras and p53 driver mutations up-regulate expression of BIRC5 [20–23]. Interestingly, our PDAC modeling using pancreatic ductal organoids revealed tumor-like morphology, demonstrating that CRISPR/Cas9 engineered organoids provide a powerful tool to recapitulate cancer development in real time [6,24,25]. Introduction of $Kras^{G12D}$ alone caused little change of morphology of ORGs in ten days with very mild expression of BIRC5, which is consistent with transformations seen in the transgenic KC mouse model [26]. However, introduction of $Kras^{G12D}$ and $p53^{Del}$ resulted in aggressive pancreatic ductal organoid morphological changes within five days, associated markedly increased BIRC5 expression. This transformation is consistent with the KPC mouse model, associated with aggressive pancreatic cancer and marked BIRC5 overexpression [26]. These data, along with published data on BIRC5 over-expression in PDAC and most solid cancers, support the selection of BIRC5 as the prototype of PDAC over-expressed gene for the feasibility study.

To achieve translation, the diagnostic platform needs to be more sensitive and specific than existing diagnostic modalities for the detection and localization of minute PDAC tumors, including currently undetectable metastases. Traditional diagnostic modalities identify larger pancreatic lesions; the diagnostic sensitivity of endoscopic ultrasound (EUS) is 95% for pancreatic tumors larger than 3 cm [27], whereas computed tomography (CT) has a sensitivity of 89%–97% with multiphasic helical detectors [28]. Endoscopic retrograde cholangiopancreatography (ERCP) and magnetic resonance cholangiopancreatography (MRCP) have a sensitivity of 86–92% [29]. However, each of these imaging modalities has poor sensitivity and specificity for minute PDAC tumors (< 10 mm) and benign precursor lesions, such as pancreatic intraepithelial neoplasm (PanIN), mucinous cystic neoplasms (MCN) and intraductal papillary mucinous neoplasms (IPMN). EUS has proven superior for detection of early pancreatic neoplasms, as compared to non-invasive imaging-based diagnostic modalities, such as CT and MRCP [30]. Only EUS with fine needle aspiration (EUS-FNA) is sufficient to definitively discriminate PDAC from other benign pancreatic lesions. However, the diagnostic accuracy of EUS-FNA is limited by several factors: it is invasive, the mass needs to be localized near the GI tract, and requires availability of onsite cytopathologists and highly skilled endoscopists [4].

Radionuclide imaging using PET reporter probes are emerging as a valuable tool for detection of cancer in small animal models and are promising for clinical applications. HSV_1-TK/[^{18}F]FHBG, a noninvasive reporter system for PET imaging, is the focus of current imaging platforms [31]. However, inability to deliver HSV_1-TK specifically to PDAC tumors has been a significant limitation [32].

Clearly, there remains an urgent need for a precision diagnostic platform that can detect and localize minute PDAC and differentiate

resectable masses from currently undetectable metastases or benign pancreatic masses. To develop the platform, we employed a four part strategy: 1. selection of BIRC5 as a PDAC overexpressed gene for generation of an enhanced BIRC5 super-promoter that would exponentially express two reporter genes; 2. selection of GLuc as a dual reporter gene, which is secreted by PDAC and therefore serologically detectable, as well as a localizing reporter in mice using optical imaging; 3. selection of a PET/CT reporter gene for localization of PDAC tumors in patients; and 4. engineering of a PDAC-specific viral delivery system. We then sought to determine whether the two reporter genes were sufficiently expressed in minute human PDAC tumors in mice using two-step amplification *via* an enhanced BIRC5 super-promoter coupled with the PDAC-specific AAV_2 delivery system. As shown in Fig. 1, minute human PDAC tumors were sensitively and specifically detected and localized in mice with serologic Gaussia luciferase (GLuc) and optical imaging, respectively, thus demonstrating feasibility of the platform. Control vectors using a CMV promoter or an AAV_2 virus lacking tumor homing peptides showed lack of specificity and considerable leakage in benign mouse tissues. There are recognized limitations of the feasibility study: 1. the human PDAC tumors were implanted subcutaneously, as opposed to orthotopic tumors; 2. human PDAC cells selected for the study express BIRC5, whereas not all PDAC tumors overexpress BIRC5; 3. BIRC5 is expressed in low levels benign human tissues.

Tumor promoter-driven reporter assays for detection of gene expression have been used previously. However, endogenous promoters are unable to detect low levels of gene expression. For this reason, we chose to utilize an enhanced super-promoter of the PDAC overexpressed gene, BIRC5. The BIRC5-SP^{TSTA} resulted in greater than 100-fold increase of promoter activity compared to endogenous BIRC5 promoter, thus it is capable of detecting low levels of BIRC5 expression in both engineered cells and PDAC cells. While synthetic promoters and the TSTA system have been studied separately [33], the strategy of combining them into an enhanced BIRC5 super-promoter for exponential reporter gene expression is novel. The limitation of using the enhanced BIRC5 super-promoter is that it could detect low levels of BIRC5 expressed in benign tissues of the human body and thus lead to false-positives. However, the magnitude of such background levels would be well-defined upon continued studies of this platform.

GLuc and sr39TK reported genes were selected for the diagnostic platform, allowing simultaneous serologic testing, optical imaging and microPET/CT imaging. While it is known that GLuc is secreted from PDAC cells and can be readily measured in blood over time, rising serologic GLuc levels correlated with increasing PDAC tumor volume, demonstrating remarkable sensitivity of serologic GLuc for detection of minute PDAC in mice [34]. The difference in blood volume between mice and humans represents a potential limitation of detection of serologic GLuc. Optical imaging is not available for clinical uses. Therefore, a PET/CT reporter gene was added to the vector for future translational purposes, as pre-clinical and clinical trials have demonstrated the feasibility of sr39TK in PET imaging of tumors [35]. Using GLuc-2A-sr39TK as a dual expression vector, we demonstrated that GLuc and sr39TK were well-cleaved without influencing their activity [36]. Quantification of [^{18}F]FHBG imaging in our study demonstrated that sr39TK localized minute human PDAC tumors bearing GLuc-2A-sr39TK in mice, therefore GLuc-2A-sr39TK serves as a single vector for simultaneous serologic detection and PET/CT localization. [^{18}F]FHBG is an ideal substrate for the HSV1-sr39TK [37]. The highly specific PDAC tumor images in this feasibility study with no visible background noise, including in the pancreas and GI tract after a clearance period of three hours, makes it suitable for imaging HSV1-sr39TK gene expression [38].

We chose AAV_2 as the delivery system, as its safety profile has long been established and it is the only FDA approved gene therapy vector available to date [16,17,39,40]. Due to non-specific limitations of AAV_2, alterations of AAV_2 tropism for cancer is an important aspect of the strategy for targeted delivery of the reporter genes [41–43]. Studies have shown that replacement of heparan sulfate proteoglycan (HSPG) on the viral capsid with high-affinity peptides permits the virus to bind specifically to tumors and prevents binding to normal cells [44,45]. Münch et al. inserted ankyrin repeat proteins specific to the HER2 receptor at the N terminus of the VP2 region of the AAV_2 capsid, thereby increasing the specificity of the vector to tumor cells overexpressing the HER2 receptor by ~30-fold *in vitro* and ~20-fold *in vivo* [45]. We genetically engineered the AAV_2 capsid with incorporation of a panel of PDAC-targeting tumor homing peptides at site R588, which have been validated to have high binding affinity to the surface membrane of tumors, thus improving viral infectivity and specificity [42,43,46]. AAV_2^{RGD} showed the highest infection of PDAC cells due to high expression of integrin αvβ3, which is consistent with other reports [44,47]. However, non-specific background signals have been observed when AAV_2^{RGD} is utilized alone due to expression of avb3 in benign tissues, therefore, AAV_2^{RGD} was coupled with the enhanced BIRC5-SP^{TSTA} to drive GLuc-2A-sr39TK dual reporter genes specifically in PDAC, as seen in Fig. 1. Conversely, the use of the wildtype AAV_2 or the engineered virus with a CMV promoter demonstrated non-specific leakage of reporter signals in benign mouse tissues. Therefore, the combination of the engineered AAV_2 and an enhanced BIRC5 super-promoter resulted in strong reporter signals only in minute human PDAC tumors with no leakage.

We recognize the future risk of administering an engineered AAV_2 to patients and thus envision that the platform would be used for patients who are undergoing high risk surgery for pancreatic cancer. Therefore, the rationale for developing the platform is to differentiate PDAC from currently undetectable metastases or benign pancreatic masses to improve surgical outcomes for patients with resectable PDAC and to avoid unnecessary surgery. We anticipate that the diagnostic platform would be used for patients who are about to undergo surgery for resectable masses of the pancreas. For example, the vector would be given one week before surgery, then the patient would undergo PET/CT imaging and serologic testing for Gaussia luciferase pre-operatively to determine whether the primary tumor is malignant or benign and whether there are metastases. If the tumor is benign or if there is metastatic disease, surgery would be avoided. One month post-operatively, serologic testing for Gaussia luciferase and PET/CT would be performed to determine whether all PDAC has been resected or whether any residual tumor or metastases are present. If the platform can reduce unnecessary surgeries by determining whether there is metastatic PDAC or benign pancreatic masses, the risk of the viral vector would be justifiable. Patients with truly resectable PDAC would experience a marked improvement in survival following surgery. The data from this feasibility study support the rationale to proceed with further studies designed for translation of the precision diagnostic platform for detecting and localizing minute human PDAC.

Conflicts of interest

The authors have no conflict of interest.

Acknowledgement

The authors would like to thank Dr. David Weaver and Allen Schroering for their technical support.

This study was supported by grants from the Moss Foundation and the Hirshberg Foundation for Pancreatic Cancer Research Fund No 58792, USA.

Appendix A. Supplementary data

Supplementary data to this article can be found online at https://doi.org/10.1016/j.canlet.2019.04.036.

References

[1] R.L. Siegel, K.D. Miller, A. Jemal, Cancer statistics, Ca - Cancer J. Clin. 67 (2017) 7–30 2017.

[2] S. Egawa, H. Toma, H. Ohigashi, T. Okusaka, A. Nakao, T. Hatori, H. Maguchi, A. Yanagisawa, M. Tanaka, Japan pancreatic cancer registry; 30th year anniversary: Japan pancreas society, Pancreas 41 (2012) 985–992.

[3] S. Bunger, T. Laubert, U.J. Roblick, J.K. Habermann, Serum biomarkers for improved diagnostic of pancreatic cancer: a current overview, J. Cancer Res. Clin. Oncol. 137 (2011) 375–389.

[4] M. Bhutani, P. Koduru, G. Lanke, M. Bruno, A. Maitra, M. Giovannini, The emerging role of endoscopic ultrasound-guided core biopsy for the evaluation of solid pancreatic masses, Minerva Gastroenterol. Dietol. 61 (2015) 51–59.

[5] P. Brader, I. Serganova, R.G. Blasberg, Noninvasive molecular imaging using reporter genes, J. Nucl. Med. 54 (2013) 167–172.

[6] S.F. Boj, C.I. Hwang, L.A. Baker, Chio II, D.D. Engle, V. Corbo, M. Jager, M. Ponz-Sarvise, H. Tiriac, M.S. Spector, A. Gracanin, T. Oni, K.H. Yu, R. van Boxtel, M. Huch, K.D. Rivera, J.P. Wilson, M.E. Feigin, D. Ohlund, A. Handly-Santana, C.M. Ardito-Abraham, M. Ludwig, E. Elyada, B. Alagesan, G. Biffi, G.N. Yordanov, B. Delcuze, B. Creighton, K. Wright, Y. Park, F.H. Morsink, I.Q. Molenaar, I.H. Borel Rinkes, E. Cuppen, Y. Hao, Y. Jin, I.J. Nijman, C. Iacobuzio-Donahue, S.D. Leach, D.J. Pappin, M. Hammell, D.S. Klimstra, O. Basturk, R.H. Hruban, G.J. Offerhaus, R.G. Vries, H. Clevers, D.A. Tuveson, Organoid models of human and mouse ductal pancreatic cancer, Cell 160 (2015) 324–338.

[7] J.F. Van Lidth de Jeude, J.L. Vermeulen, P.S. Montenegro-Miranda, G.R. Van den Brink, J. Heijmans, A protocol for lentiviral transduction and downstream analysis of intestinal organoids, J. Vis. Exp. 98 (2015) 52531.

[8] R.J. Platt, S. Chen, Y. Zhou, M.J. Yim, L. Swiech, H.R. Kempton, J.E. Dahlman, O. Parnas, T.M. Eisenhaure, M. Jovanovic, D.B. Graham, S. Jhunjhunwala, M. Heidenreich, R.J. Xavier, R. Langer, D.G. Anderson, N. Hacohen, A. Regev, G. Feng, P.A. Sharp, F. Zhang, CRISPR-Cas9 knockin mice for genome editing and cancer modeling, Cell 159 (2014) 440–455.

[9] K. Satoh, K. Kaneko, M. Hirota, A. Masamune, A. Satoh, T. Shimosegawa, Expression of survivin is correlated with cancer cell apoptosis and is involved in the development of human pancreatic duct cell tumors, Cancer 92 (2001) 271–278.

[10] M. Jinfeng, W. Kimura, F. Sakurai, T. Moriya, A. Takeshita, I. Hirai, Histopathological study of intraductal papillary mucinous tumor of the pancreas: special reference to the roles of Survivin and p53 in tumorigenesis of IPMT, Int. J. Gastrointest. Cancer 32 (2002) 73–81.

[11] A.I. Sarela, C.S. Verbeke, J. Ramsdale, C.L. Davies, A.F. Markham, P.J. Guillou, Expression of survivin, a novel inhibitor of apoptosis and cell cycle regulatory protein, in pancreatic adenocarcinoma, Br. J. Canc. 86 (2002) 886–892.

[12] J. Dehairs, A. Talebi, Y. Cherifi, J.V. Swinnen, CRISP-ID: decoding CRISPR mediated indels by Sanger sequencing, Sci. Rep. 6 (2016) 28973.

[13] S.H. Liu, J. Yu, R. Sanchez, X. Liu, D. Heidt, J. Willey, J. Nemunaitis, F.C. Brunicardi, A novel synthetic human insulin super promoter for targeting PDX-1-expressing pancreatic cancer, Cancer Lett. 418 (2018) 75–83.

[14] R. Boidot, F. Vegran, S. Lizard-Nacol, Transcriptional regulation of the survivin gene, Mol. Biol. Rep. 41 (2014) 233–240.

[15] M. Iyer, L. Wu, M. Carey, Y. Wang, A. Smallwood, S.S. Gambhir, Two-step transcriptional amplification as a method for imaging reporter gene expression using weak promoters, Proc. Natl. Acad. Sci. U. S. A. 98 (2001) 14595–14600.

[16] M. Niethammer, C.C. Tang, P.A. LeWitt, A.R. Rezai, M.A. Leehey, S.G. Ojemann, A.W. Flaherty, E.N. Eskandar, S.K. Kostyk, A. Sarkar, M.S. Siddiqui, S.B. Tatter, J.M. Schwalb, K.L. Poston, J.M. Henderson, R.M. Kurlan, I.H. Richard, C.V. Sapan, D. Eidelberg, M.J. During, M.G. Kaplitt, A. Feigin, Long-term follow-up of a randomized AAV2-GAD gene therapy trial for Parkinson's disease, JCI Insight 2 (2017) e90133.

[17] W.A. Beltran, A.V. Cideciyan, S.E. Boye, G.J. Ye, S. Iwabe, V.L. Dufour, L.F. Marinho, M. Swider, M.S. Kosyk, J. Sha, S.L. Boye, J.J. Peterson, C.D. Witherspoon, J.J. Alexander, G.S. Ying, M.S. Shearman, J.D. Chulay, W.W. Hauswirth, P.D. Gamlin, S.G. Jacobson, G.D. Aguirre, Optimization of retinal gene therapy for X-linked retinitis pigmentosa due to RPGR mutations, Mol. Ther. 25 (2017) 1866–1880.

[18] F. Danhier, A. Le Breton, V. Preat, RGD-based strategies to target alpha(v) beta(3) integrin in cancer therapy and diagnosis, Mol. Pharm. 9 (2012) 2961–2973.

[19] M.J. Duffy, N. O'Donovan, D.J. Brennan, W.M. Gallagher, B.M. Ryan, Survivin: a promising tumor biomarker, Cancer Lett. 249 (2007) 49–60.

[20] K.W. Sommer, C.J. Schamberger, G.E. Schmidt, S. Sasgary, C. Cerni, Inhibitor of apoptosis protein (IAP) survivin is upregulated by oncogenic c-H-Ras, Oncogene 22 (2003) 4266–4280.

[21] D. Raj, T. Liu, G. Samadashwily, F. Li, D. Grossman, Survivin repression by p53, Rb and E2F2 in normal human melanocytes, Carcinogenesis 29 (2008) 194–201.

[22] W.H. Hoffman, S. Biade, J.T. Zilfou, J. Chen, M. Murphy, Transcriptional repression of the anti-apoptotic survivin gene by wild type p53, J. Biol. Chem. 277 (2002) 3247–3257.

[23] R. Hadj-Slimane, P. Pamonsinlapatham, J.P. Herbeuval, C. Garbay, Y. Lepelletier, F. Raynaud, RasV12 induces Survivin/AuroraB pathway conferring tumor cell apoptosis resistance, Cell. Signal. 22 (2010) 1214–1221.

[24] M. Huch, B.K. Koo, Modeling mouse and human development using organoid cultures, Development 142 (2015) 3113–3125.

[25] J. Drost, H. Clevers, Organoids in cancer research, Nat. Rev. Canc. 18 (2018) 407–418.

[26] C.B. Westphalen, K.P. Olive, Genetically engineered mouse models of pancreatic cancer, Cancer J. 18 (2012) 502–510.

[27] B.M. Karlson, A. Ekbom, P.G. Lindgren, V. Kallskog, J. Rastad, Abdominal US for diagnosis of pancreatic tumor: prospective cohort analysis, Radiology 213 (1999) 107–111.

[28] C. Valls, E. Andia, A. Sanchez, J. Fabregat, O. Pozuelo, J.C. Quintero, T. Serrano, F. Garcia-Borobia, R. Jorba, Dual-phase helical CT of pancreatic adenocarcinoma: assessment of resectability before surgery, AJR Am. J. Roentgenol. 178 (2002) 821–826.

[29] J.C. Varghese, M.A. Farrell, G. Courtney, H. Osborne, F.E. Murray, M.J. Lee, Role of MR cholangiopancreatography in patients with failed or inadequate ERCP, AJR Am. J. Roentgenol. 173 (1999) 1527–1533.

[30] E.J. Shin, M. Topazian, M.G. Goggins, S. Syngal, J.R. Saltzman, J.H. Lee, J.J. Farrell, M.I. Canto, Linear-array EUS improves detection of pancreatic lesions in high-risk individuals: a randomized tandem study, Gastrointest. Endosc. 82 (2015) 812–818.

[31] S.S. Yaghoubi, M.C. Jensen, N. Satyamurthy, S. Budhiraja, D. Paik, J. Czernin, S.S. Gambhir, Noninvasive detection of therapeutic cytolytic T cells with 18F-FHBG PET in a patient with glioma, Nat. Clin. Pract. Oncol. 6 (2009) 53–58.

[32] S.S. Yaghoubi, M.A. Couto, C.C. Chen, L. Polavaram, G. Cui, L. Sen, S.S. Gambhir, Preclinical safety evaluation of 18F-FHBG: a PET reporter probe for imaging herpes simplex virus type 1 thymidine kinase (HSV1-tk) or mutant HSV1-sr39tk's expression, J. Nucl. Med. 47 (2006) 706–715.

[33] M. Iyer, F.B. Salazar, X. Lewis, L. Zhang, L. Wu, M. Carey, S.S. Gambhir, Non-invasive imaging of a transgenic mouse model using a prostate-specific two-step transcriptional amplification strategy, Transgenic Res. 14 (2005) 47–55.

[34] B.A. Tannous, Gaussia luciferase reporter assay for monitoring biological processes in culture and in vivo, Nat. Protoc. 4 (2009) 582–591.

[35] S.S. Gambhir, E. Bauer, M.E. Black, Q. Liang, M.S. Kokoris, J.R. Barrio, M. Iyer, M. Namavari, M.E. Phelps, H.R. Herschman, A mutant herpes simplex virus type 1 thymidine kinase reporter gene shows improved sensitivity for imaging reporter gene expression with positron emission tomography, Proc. Natl. Acad. Sci. U. S. A. 97 (2000) 2785–2790.

[36] Z. Liu, O. Chen, J.B.J. Wall, M. Zheng, Y. Zhou, L. Wang, H. Ruth Vaseghi, L. Qian, J. Liu, Systematic comparison of 2A peptides for cloning multi-genes in a polycistronic vector, Sci. Rep. 7 (2017) 2193.

[37] S.S. Yaghoubi, J.R. Barrio, M. Namavari, N. Satyamurthy, M.E. Phelps, H.R. Herschman, S.S. Gambhir, Imaging progress of herpes simplex virus type 1 thymidine kinase suicide gene therapy in living subjects with positron emission tomography, Cancer Gene Ther. 12 (2005) 329–339.

[38] J. Yong, J. Rasooly, H. Dang, Y. Lu, B. Middleton, Z. Zhang, L. Hon, M. Namavari, D.B. Stout, M.A. Atkinson, J. Tian, S.S. Gambhir, D.L. Kaufman, Multimodality imaging of beta-cells in mouse models of type 1 and 2 diabetes, Diabetes 60 (2011) 1383–1392.

[39] W. San Sebastian, A.P. Kells, J. Bringas, L. Samaranch, P. Hadaczek, A. Ciesielska, M. Macayan, P.J. Pivirotto, J. Forsayeth, S. Osborne, J.F. Wright, F. Green, G. Heller, K.S. Bankiewicz, Safety and tolerability of MRI-guided infusion of AAV2-hAADC into the mid-brain of non-human primate, Mol. Ther. Methods Clin. Dev. 3 (2014).

[40] D.E. Bowles, S.W. McPhee, C. Li, S.J. Gray, J.J. Samulski, A.S. Camp, J. Li, B. Wang, P.E. Monahan, J.E. Rabinowitz, J.C. Grieger, L. Govindasamy, M. Agbandje-McKenna, X. Xiao, R.J. Samulski, Phase 1 gene therapy for Duchenne muscular dystrophy using a translational optimized AAV vector, Mol. Ther. 20 (2012) 443–455.

[41] L. Perabo, D. Goldnau, K. White, J. Endell, J. Boucas, S. Humme, L.M. Work, H. Janicki, M. Hallek, A.H. Baker, H. Buning, Heparan sulfate proteoglycan binding properties of adeno-associated virus retargeting mutants and consequences for their in vivo tropism, J. Virol. 80 (2006) 7265–7269.

[42] T.F. Lerch, M.S. Chapman, Identification of the heparin binding site on adeno-associated virus serotype 3B (AAV-3B), Virology 423 (2012) 6–13.

[43] A.L. Arnett, L.R. Beutler, A. Quintana, J. Allen, E. Finn, R.D. Palmiter, J.S. Chamberlain, Heparin-binding correlates with increased efficiency of AAV1- and AAV6-mediated transduction of striated muscle, but negatively impacts CNS transduction, Gene Ther. 20 (2013) 497–503.

[44] W. Shi, J.S. Bartlett, RGD inclusion in VP3 provides adeno-associated virus type 2 (AAV2)-based vectors with a heparan sulfate-independent cell entry mechanism, Mol. Ther. 7 (2003) 515–525.

[45] R.C. Munch, H. Janicki, I. Volker, A. Rasbach, M. Hallek, H. Buning, C.J. Buchholz, Displaying high-affinity ligands on adeno-associated viral vectors enables tumor cell-specific and safe gene transfer, Mol. Ther. 21 (2013) 109–118.

[46] M. Mietzsch, F. Broecker, A. Reinhardt, P.H. Seeberger, R. Heilbronn, Differential adeno-associated virus serotype-specific interaction patterns with synthetic heparins and other glycans, J. Virol. 88 (2014) 2991–3003.

[47] M. Ruffing, H. Heid, J.A. Kleinschmidt, Mutations in the carboxy terminus of adeno-associated virus 2 capsid proteins affect viral infectivity: lack of an RGD integrin-binding motif, J. Gen. Virol. 75 (Pt 12) (1994) 3385–3392.